E3S Web of Conferences **504**, 02001 (2024) https://doi.org/10.1051/e3sconf/202450402001
Journées Scientifiques AGAP Qualité 2024

Passive seismic tomography for 3D imaging of the subsurface in a tunnel area

Tomographie sismique passive pour imager en 3D le sous-sol dans une zone de tunnels

Maria Saade[1*], *Simon* Robert[1], *Clément* Lempereur[1], and *Michel* Grill[2]

[1]Geophysics group, Sixense Engineering, 22 rue Lavoisier, 92000 Nanterre, France
[2]Sixense In-Situ, 5 rue Geespelt, L-3378 Livange - Luxembourg

Abstract. This study aims to provide decision support for future measures to be taken regarding 2 tunnels using high-resolution 3D imaging of the subsurface. This project involves a more comprehensive risk analysis than localized tests, such as geotechnical surveys, and a more precise characterization of the subsoil at the tunnel entrance for approximately 200 meters. To address this issue, a 3D passive seismic tomography was conducted using a network installed on the surface of the study area and another in the tunnels to better analyze the subsurface beneath the tunnels. The 3D shear wave velocity model allowed the identification and delineation of risk zones and the estimation of risk levels based on the analysis of Vs (shear wave velocity) contrasts and their correlation with borehole data.

Résumé. Cette étude a pour but d'apporter une aide à la décision sur les futures dispositions à prendre au niveau de 2 tunnels à l'aide d'une imagerie 3D haute résolution du sous-sol. Ce projet consiste d'une analyse de risques plus étendue que des essais localisés, tels que les sondages géotechniques, et une caractérisation plus précise des terrains de l'entrée de tunnels à environ 200 m de long. Afin de répondre à cette problématique, une tomographie 3D en sismique passive a été réalisé à partir d'un réseau installé sur la surface de la zone d'étude et un autre dans les tunnels afin d'avoir une meilleure analyse du sous-sol au-dessous des tunnels. Le modèle 3D de vitesse de cisaillement a permis la localisation et la délimitation de zones à risques et l'estimation du niveau de risque à partir de l'analyse des contrastes de Vs et la corrélation aux sondages.

1 Context and objectives

The study site is located around the 2 tubes of the Markusbierg tunnel towards the German side (see Figure below).

* Corresponding author: maria.saade@vinci-construction.fr

Fig. 1. On the left: Seismic network on the surface. On the right: Seismic network in the tunnels. The red and yellow dots represent the location of the seismic nodes.

According to a geological cross-section the study area consists of: Keuper with marlstone layers and Gypsum marls and passages of gypsum and anhydrite.
Some land subsidence was observed in the tunnel mainly at the entrance. The localisation and delimitation of the soil at risk is difficult with 1D localised techniques such as geotechnical surveys. The purpose of this study was then to analyse the sub-soil around the tunnels with a 3D high resolution tomography, that allows a complete imagery of the sub-soil, to assess the areas at risk, better localise soil treatment and/or help for the decision of tunnels reconstruction.

The solution is a 3D tomography using ambient noise interferometry. For this purpose, 199 autonomous sensors were deployed on the surface (see Figure 1) and 50 sensors in the tunnels (see Figure 1).

2 Technique and Results

2.1 Passive Seismic Tomography and Measurements

Passive seismic tomography is a technique used to explore (image and monitor) the subsurface using ambient noise generated by natural or anthropogenic sources [1, 2, 5, 7, 9, 10]. The method is based on calculating the cross-correlations of the noise signal between two seismic sensors. The noise is dominated by surface waves propagating in the shallow crust [6, 8]. From the cross-correlations, the following can be extracted:

1- The Green's function between two sensors A and B [3, 4, 11, 12], that represents the impulse response of the medium between these two points. Consequently, the seismic velocity in the area between A and B can be extracted.
2- Dispersion curves of surface waves, presented in the form of a diagram representing variations in velocity as a function of frequency. Indeed, the propagation velocity of surface waves depends on the shear wave velocity (Vs). Their penetration depth is proportional to their wavelength.

To ensure the operation of the sensors in tunnels that require a GPS network, GPS signal repeaters have been installed in the two tunnels. The distance between the repeaters is approximately 40 to 50 m. These repeaters are connected to each other and to an antenna fixed outside.

For this study, 199 surface sensors are used, covering the study area with a variable inter-sensor distance averaging about 20 m. Additionally, 50 sensors are installed inside the two

tunnels to image the subsoil beneath them more finely (with an average inter-sensor distance of 10 m).

Approximately 336 hours of measurements were recorded by 199 surface sensors and 672 hours by the 50 sensors in the tunnel.

A total of 19900 cross-correlations (CC) of continuous noise signal is calculated between the 199 surface sensors, and 903 CC are calculated between the 50 tunnel sensors. This number is equivalent to the number of sensor pairs and, therefore, the number of velocity measurements obtained. The CCs are calculated hour by hour throughout the acquisition period and for all sensor pairs. Subsequently, the CCs are averaged for each sensor pair over the entire listening period, improving the signal-to-noise ratio of the CCs and highlighting the surface wave. It is noteworthy that surface and tunnel data are processed separately, as it is not possible to calculate a cross-correlation between a surface sensor and a tunnel sensor due to significant differences in altitude. The combination of surface and tunnel results occurs during the visualization stage of the 3D blocks obtained through tomography.

The calculation of cross-correlation between 2 sensors allows the extraction of the surface wave contained in the noise propagating between these 2 sensors. The cross-correlation signal is centred at zero. The positive part is equivalent to the seismic signal propagating from the 1st sensor to the 2nd sensor, and the negative part corresponds to the signal propagating from the 2nd sensor to the 1st sensor. From this mathematical procedure, the surface wave is extracted, and the velocity between the 2 sensors is calculated based on the propagation time (dt) of the wave measured on the cross-correlation.

Dispersion curves are then computed. Thus, for each sensor pair, variations in velocity are obtained based on frequency.

The dispersion curves are inverted in the frequency band of 2 to 20 Hz to obtain variations in shear velocity (Vs) as a function of depth for each sensor pair. With the dense sensor network in place, two 3D images of the Vs distribution are then obtained: one image from surface data covering from the surface to 50 m depth, and another from tunnel data spanning from the tunnels to 15 m below the tunnels. The final misfit of the inversion is homogeneous and low with an average of 7%.

2.2 Description and Interpretation of the results

The analysis of measurements allows obtaining a 3D model of shear velocities (see Figure 2). The maps below are excerpts from this velocity model. The horizontal resolution of the 3D model depends on the sensor distribution and is equivalent to the inter-sensor spacing. In a less dense sensor area, the model resolution is lower. The vertical resolution is more challenging to quantify, as it depends on several parameters, but it degrades with depth.

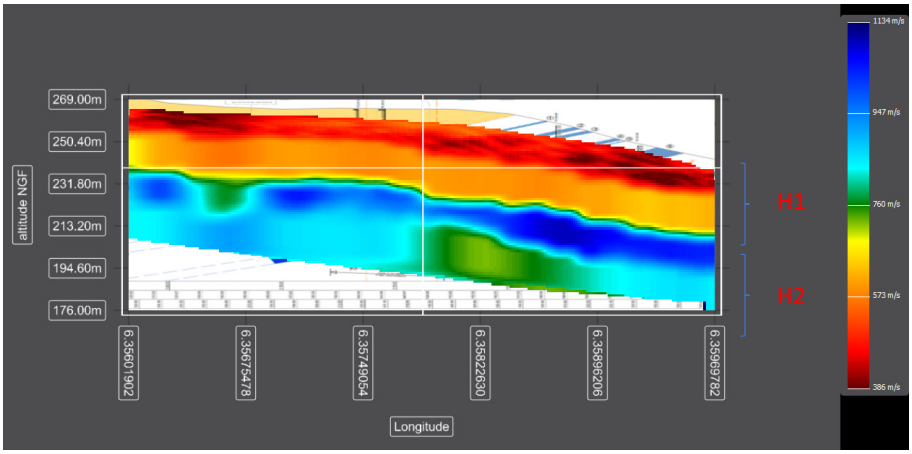

Fig. 2. 3D shear velocity model obtained with surface data.

It is worth recalling that the study's objective is to analyse the overall quality of the subsurface and identify significant velocity contrasts that can be interpreted by the presence of more fractured material, cavities, etc.

Note that a seismic horizon does not necessarily correspond to a geological horizon. Seismic velocities indicate contrasts in material density, considering that two geological horizons can have the same density. A velocity contrast less than the misfit (average of 7%) is not necessarily interpretable.

In general, and based on the results obtained, the following information has been noted:

- Shear velocity values throughout the study area vary between approximately 300 and 1200 m/s in the first 50 meters of depth.
- The 3D model of surface data highlights 2 main seismic horizons (see Figure 2) centred around velocities of 650 m/s and 950 m/s, with significant lateral variations in each horizon. The analysis aims to identify velocity contrasts in these 2 seismic horizons that exceed the measurement uncertainty value.
- The 3D model of surface and tunnel data also highlights 2 relatively lower velocity zones (Fig. 11 and 12), which will be detailed later.
- A main interface is highlighted at a depth of approximately 20 meters. This interface separates the layer of velocities ranging from 300 to 700 m/s (red and yellow layer, likely dominated by the presence of Keuper) and the layer of velocities exceeding 700 m/s (blue layer, probably dominated by the presence of gypsum-rich marls). Velocities gradually increase with depth. These higher velocities seem to indicate the presence of relatively more competent, massive, or rocky materials, or materials with lower permeability than the Keuper.

Description of the high-velocity-contrast zones surrounded in red in Figures 3 and 4:

Two velocity-contrast zones of approximately 25% are identified within the homogeneity of Horizon 2. This represents a velocity decrease beyond the error range (average of 7%), but it does not necessarily imply a significant change in material quality. As a reminder, a decrease in shear velocity is linked to a decrease in the intrinsic density of the material. This can be attributed either to a material change or to a higher degree of alteration of the same material.

The first contrast zone is located at the entrance of the tunnel (area surrounded in red on the right in Figures 3 and 4), where a karstic conduit had been observed. It is observable from a depth of 20 m to the model limit and extends over a length of approximately 80 m.

An unclosed anomaly to the west, of unknown origin, is also observed and surrounded in red on the left in Figures 3 and 4.

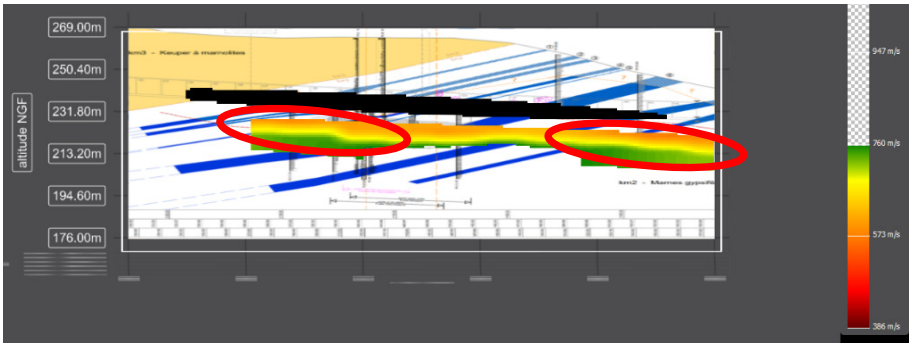

Fig. 3. 3D shear velocity model obtained with tunnel data. Low velocity filter applied (< 700 m/s) on the model to highlight Horizon 1 and focus on the altered material.

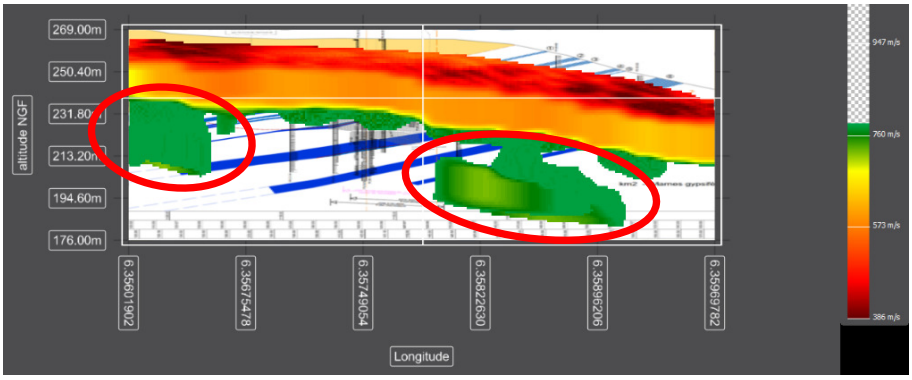

Fig. 4. 3D shear velocity model obtained with surface data. Low velocity filter applied on the model to highlight Horizon 1.

Description of the positive-velocity-contrast zone surrounded in red in Figure 5 and highlighted in Figure 6:

A positive velocity anomaly, reaching up to 35%, is observed below the tunnels (throughout the investigation depth, 30 m or more). This anomaly is located at the site of anchorages and injections and can therefore be explained by the improvement in soil quality due to injection works.

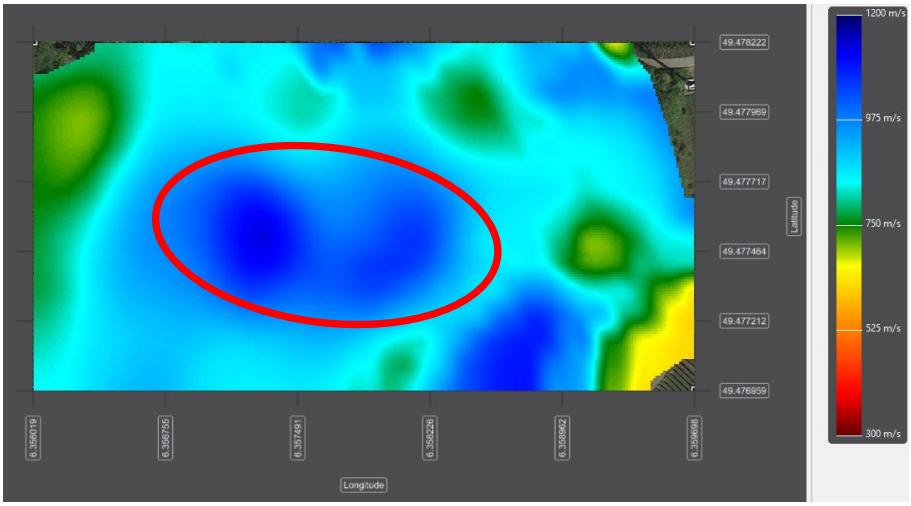

Fig. 5. Horizontal section of the shear velocity model obtained from surface data at approximately 45-50 m.

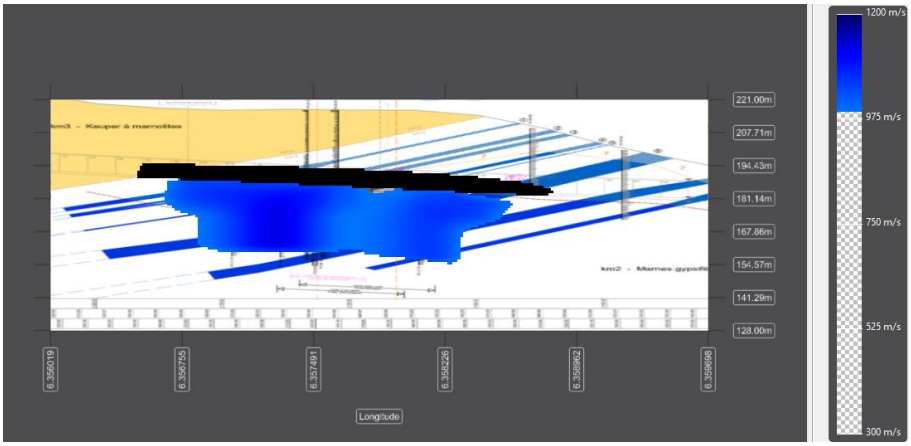

Fig. 6. Vertical section of the shear velocity model obtained from surface data at the location of the descending tube (P-S) of the tunnels. Filter for high velocities (> 975 m/s) applied in order to highlight relatively denser material.

3 Conclusion

The study aimed to visualize the subsurface around the Markusbierg tunnel, from the tunnel entrance on the German side, covering approximately 200 meters in length.

The passive seismic tomography allowed to image the subsurface in 3D at a relatively high resolution and with a non-invasive acquisition. Areas at risk were identified and delimited, in the whole area of study.

In the 3D models of Vs, two seismic horizons are identified that are comparable to drilling results and geological layers but exhibit varied degrees of material alteration. At the tunnel

entrances, a zone with a higher degree of material alteration is more pronounced, reaching an average of 25%. Another anomaly zone is also identified at the extreme west of the model.

To determine the nature of these anomalies, it is possible to rely on the results of core drilling as well as on the surfaces defined previously by the contour of anomalies with lower seismic velocities Vs from the 3D model (Zone of velocity anomaly Vs <700 m/s), which are potentially the most unfavourable in terms of cavity risk or the presence of more fractured or altered terrains.

References

1. Brenguier, F., N. M. Shapiro, M. Campillo, A. Nercessian, and V.Ferrazzini, 3-D surface wave tomography of the Piton de la Fournaise volcano using seismic noise correlations, Geophys. Res. Lett., 34, L02305, doi:10.1029/2006GL028586 (2007).
2. Brenguier, F., N. M. Shapiro, M. Campillo, A. Nercessian, and V.Ferrazzini, 3-D surface wave tomography of the Piton de la Fournaise volcano using seismic noise correlations, Geophys. Res. Lett., 34, L02305, doi:10.1029/2006GL028586 (2007).
3. Duvall, T., Jefferies, S., Harvey, J. & Pomerantz, M. Time–distance helioseismology, Nature, 362, 430–432 (1993).
4. Gouédard, P. et al. Cross-correlation of random fields: mathematical approach and applications, Geophys. Prospect., 56(3), 375–393 (2008).
5. Mordret, A., N. M. Shapiro, S. Singh, P. Roux, and O. I. Barkved, Helmholtz Tomography of ambient noise surface wave data to estimate Scholte wave phase velocity at Valhall Life of the Field, Geophysics, 78(2), WA99–WA109. doi: 10.1190/geo2012-0303.1 (2013).
6. Roux, P., Antoine Roueff and Marc Wathelet, The San Andreas Fault revisited through seismic-noise and surface-wave tomography, Geophys. Res. Lett., 38, L13319, (2011).
7. Sabra, K., Gerstoft, P., Roux, P., Kuperman,W. & Fehler, M. Surface wave tomography from microseisms in Southern California, Geophys. Res. Lett., 32, L14311, doi:10.1029/2005GL023155 (2005).
8. Shapiro N.M., and M. Campillo, Emergence of broadband Rayleigh waves from correlations of the ambient seismic noise, Geophys. Res. Letters, VOL. 31, L07614, doi:10.1029/2004GL019491 (2004).
9. Shapiro, NM, M. Campillo, L. Stehly and M. Ritzwoller, High Resolution Surface-Wave Tomography from Ambient Seismic Noise, Science, 307, 1615-1618 (2005).
10. Olivier. G., F. Brenguier, M. Campillo, P. Roux, N. M. Shapiro, R. Lynch, Investigation of co- and post-seismic processes with in-situ measurements of seismic velocity variations in an underground mine, Geophys. Res. Letters (2015).
11. Wapenaar, K. Retrieving the elastodynamic Green's function of an arbitrary inhomogeneous medium by cross correlation, Phys. Rev. Lett., 93(25), 254301, doi:10.1103/PhysRevLett.93.254301 (2004).
12. Weaver, R. & Lobkis, O. Ultrasonics without a source: thermal fluctuation correlations at MHz frequencies, Phys. Rev. Lett., 87(13), 134301, doi:10.1103/PhysRevLett.87.134301. Webb, S., 1998. Broadband seismology (2001)